

## Evaporation Induced Vertical Alignment Enabling Directional Ion Transport in 2D Nanosheet-Based Battery Electrode

*Yue Zhu, Zhengyu Ju, Xiao Zhang, Diana M. Lutz, Lisa M. Housel, Yangen Zhou, Kenneth J. Takeuchi, Esther S. Takeuchi, Amy C. Marschilok, and Guihua Yu\**

Y. Zhu, Z. Ju, X. Zhang, Dr. Y. Zhou, Prof. G. Yu

Materials Science and Engineering Program

Texas Materials Institute

The University of Texas at Austin

Austin, TX 78712, USA

E-mail: [ghyu@austin.utexas.edu](mailto:ghyu@austin.utexas.edu)

D. M. Lutz, L. M. Housel, Prof. K. Takeuchi, Prof. E. Takeuchi, Prof. A. Marschilok

Department of Chemistry

Stony Brook University

Stony Brook, NY 11794, USA

Prof. E. Takeuchi, Prof. A. Marschilok

Energy and Photon Sciences Directorate

Brookhaven National Laboratory

Upton, NY 11973, USA

This is the author manuscript accepted for publication and has undergone full peer review but has not been through the copyediting, typesetting, pagination and proofreading process, which may lead to differences between this version and the [Version of Record](#). Please cite this article as [doi: 10.1002/adma.201907941](https://doi.org/10.1002/adma.201907941).

This article is protected by copyright. All rights reserved.

Prof. K. Takeuchi, Prof. E. Takeuchi, Prof. A. Marschilok

Department of Materials Science and Chemical Engineering

Stony Brook University

Stony Brook, NY 11794, USA

Manuscript  
Author

Two-dimensional (2D) nanosheets have been widely explored as electrode materials owing to their extraordinarily high electrochemical activity and fast solid-state diffusion. However, the scalable electrode fabrication based on this type of materials usually suffers from severe performance losses due to restricted ion transport kinetics in large thickness. Here, a novel strategy based on evaporation-induced assembly to enable directional ion transport via forming vertically aligned nanosheets is reported. The orientation ordering is achieved by a rapid evaporation of mixed solvents during the electrode fabrication process. Compared with conventional drop-casted electrodes, which exhibit a random arrangement of the nanosheets and obvious decrease of rate performance with increasing thickness, the vertically aligned nanosheets electrode is able to retain the original high rate capability even at high mass loadings and electrode thickness. Combined electrochemical and structural characterizations reveal the electrode composed of orientation controlled nanosheets to possess lower charge transfer resistances, leading to more complete phase transformation in the active materials.

The success of Lithium-ion batteries (LIBs) in powering consumer electronic devices and electrifying the transportation sector has stimulated considerable research interest in exploring new materials and structures that meet the ever-increasing technological demand for higher density and more rapid energy storage.<sup>[1]</sup> Besides the efforts to exploit synthetic and engineering methods toward high performance materials and advantageous structures,<sup>[2]</sup> equally critical is the development of scalable manufacturing of thick electrode to achieve high loading of active material without compromising power density.<sup>[3]</sup> This direction of research requires scientific knowledge in assembly of materials with ion- and electron-conducting phases, understanding of multiscale transport processes, and rational design of composite architectures optimizing the electrode kinetics.<sup>[4]</sup>

This article is protected by copyright. All rights reserved.

Many newly explored electrochemical active materials with ultrathin 2D morphology and tunable interlayer structure have been demonstrated to show promising properties toward energy storage applications.<sup>[5]</sup> However, there are several key scientific hurdles that must be overcome to allow these materials to fulfill their full promise. For instance, 2D nanosheets usually suffer from diminished performance when fabricated into thick electrode films.<sup>[6]</sup> At the heart of this issue is the lack of suitable fabrication methods to replace traditional ones that often lead to restacking of 2D nanosheets. Several strategies exist to facilitate ion transport throughout the entire film thickness by introducing nanoscale porosity or microscale vertical channels,<sup>[7]</sup> and their applications to 2D nanosheet-based electrode have been recently demonstrated.<sup>[8]</sup> But such mitigation strategies tend to produce electrodes with relatively low volumetric energy density due to the unnecessary porosity or void generated.

An intriguing property of 2D nanosheets is their large aspect ratio, which could be exploited to form various structures with desired orientation, exhibiting superior material properties over their randomly arranged counterparts.<sup>[9]</sup> This manipulation of the macroscopic assembly state is particularly useful to produce dense films in a controlled and scalable manner. For example, thick films based on vertically aligned 2D Mxene nanosheets have been shown to facilitate directional ion transport that lead to thickness-independent electrochemical performances.<sup>[9b]</sup> In comparison with strategies that enable similar directional transport mechanism, for instance, ice-templating method, the main advantage by direct tuning orientation of the nanosheets is the resulting compact structure without excessive void space. Despite the success of such self-assembly approach presented in Mxene system, this approach remains challenging to be extended to other 2D nanosheets due to the required formation of a unique liquid-crystalline phase and the associated multistep fabrication processes. Nevertheless, the demonstrated high rate performance enabled by vertical alignment

manifests the importance of precise control of directional ion transport in nanosheet-based thick electrodes.

In a conventional electrode preparation process, a slurry of a mixture containing active material, conductive carbon and other additives in a solvent is casted onto the current collector and allowed to dry. While much attention is focused on the slurry itself, such as the ratio of between each component and the role of additive, the drying process has not been fully utilized to control electrode architectures. During evaporation of the solvent, particles of active material gradually precipitate and arrange themselves according to the minimum energy configuration.<sup>[10]</sup> If the evaporation process is extremely rapid, the arrangement of active material may be kinetically affected and the final configuration may essentially freeze into a thermodynamically unfavored state. The feasibility of using solvent evaporation toward ordered and oriented structures has been well established in several anisotropic nanomaterials, for example, gold nanorods.<sup>[11]</sup> Inspired by this concept, in this work, we used ultrathin VOPO<sub>4</sub> nanosheets (Figure S1, Supporting Information) as a model material<sup>[12]</sup> to demonstrate a facile fabrication method to achieve orientation control in the evaporation process. We found that almost-randomly arranged nanosheets with slightly preferred horizontal stacking would be the representative morphology using the conventional fabrication method (Figure 1a). Intriguingly, a dense film of vertically aligned nanosheets (VANS) could be produced after rapid drying of the slurry prepared in a mixed solvent (Figure 1b). The assembly of nanosheets on an electrode with a vertical alignment configuration highlights a low tortuosity structure for efficient ion transport, which is absent in the stacked nanosheets on a conventional electrode.

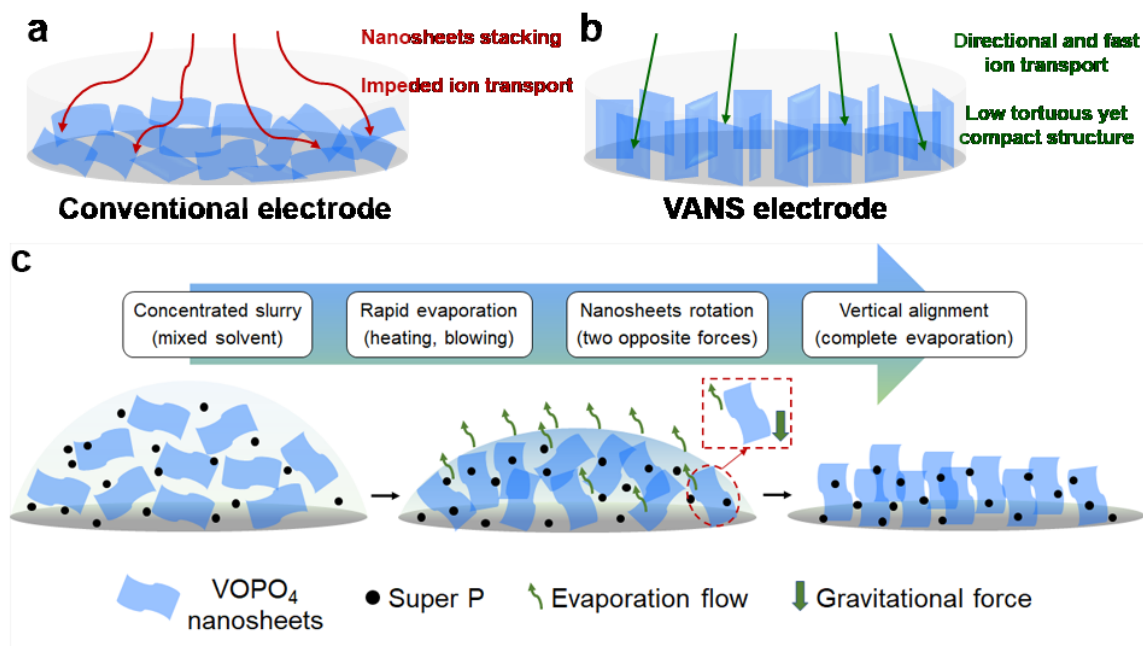


**Figure 1.** Schematic illustration of assemblies of VOPO<sub>4</sub> nanosheets and associated transport characteristics in a) conventionally made electrode with random arrangement and b) VANS electrode with vertical alignment. c) Key steps in the solvent evaporation induced alignment method used in this work.

The key to success for orientational ordering lies in the controlled evaporation process (Methods, Supporting Information) and associated alignment mechanism. As depicted in Figure 1c, a typical VANS electrode fabrication process starts with a slurry composed of a concentrated suspension of 2D VOPO<sub>4</sub> nanosheets and spherical Super P as the carbon additive in a mixed solvent, necessary for success. Rapid solvent evaporation is enabled by heating and evacuating the air over the electrode (Figure S2, Supporting Information), leading to quick shrinkage of the slurry volume with an associated increase in concentration. During this process, the nanosheets experience two opposite forces, the downward gravitational force and an upward force induced by the evaporation

flow. As a result of the net torque from the two forces, the nanosheets rotate clockwise until they become vertically aligned with respect to the current collector. Though being a product of the kinetic process, the majority of the nanosheets maintain a vertical configuration as there is insufficient relaxation time for them to reach a more thermodynamically stable state of laying flat, leading to formation of the VANS electrode.

The rational selection of  $\text{VOPO}_4$  material in this study is based on its unique structural characteristics and associated electrochemical properties. The 2D layered structure of  $\text{VOPO}_4$  is composed of interconnected  $\text{VO}_6$  octahedra and  $\text{PO}_4$  tetrahedra, containing active vanadium centers with a high redox potential (**Figure 2a**). More importantly, its relatively large interlayer distance due to the existence of interlayer water molecules features high-rate electrochemical storage through intercalation pseudocapacitance mechanism.<sup>[12b]</sup> The liquid exfoliation of bulk microcrystals produces a stable and processable solution (**Figure 2b**), showing well dispersed nanosheets (**Figure 2c**) as imaged by scanning electron microscopy (SEM). A close look at an individual nanosheet by transmission electron microscopy (TEM) reveals its ultrathin thickness (**Figure 2d**), and the corresponding selected area electron diffraction (SAED) pattern (**Figure 2e**) confirms the single crystallinity after exfoliation. The conventional electrode made by the standard drop-casting method exhibits no obvious ordering in the nanosheets except that they are mostly lying facing up, as shown by the top view of the electrode (**Figure 2f**). Consistently, the side view image (**Figure 2g**) also indicates the nanosheets are horizontally stacked as expected from their large aspect ratio, though not in a highly compact configuration possibly due to the presence of the spherical carbon additive. In contrast, the VANS electrode clearly shows that the majority of the nanosheets are aligned vertically, as viewed from both the top (**Figure 2h**) and side of the electrode (**Figure 2i and j**). The different arrangements of the nanosheets on the electrodes are also reflected in their corresponding

X-ray diffraction (XRD) patterns (Figure 2k), in which the ratio of peak intensities for the basal and edge planes varies according to the preferred orientation.<sup>[9c]</sup> For horizontal arrangement of the nanosheets with basal planes facing up, (001) peak shows the highest intensity. While in vertical arrangement, the largely exposed edge planes cause intensity of (200) peak to be significantly higher than that of (001).

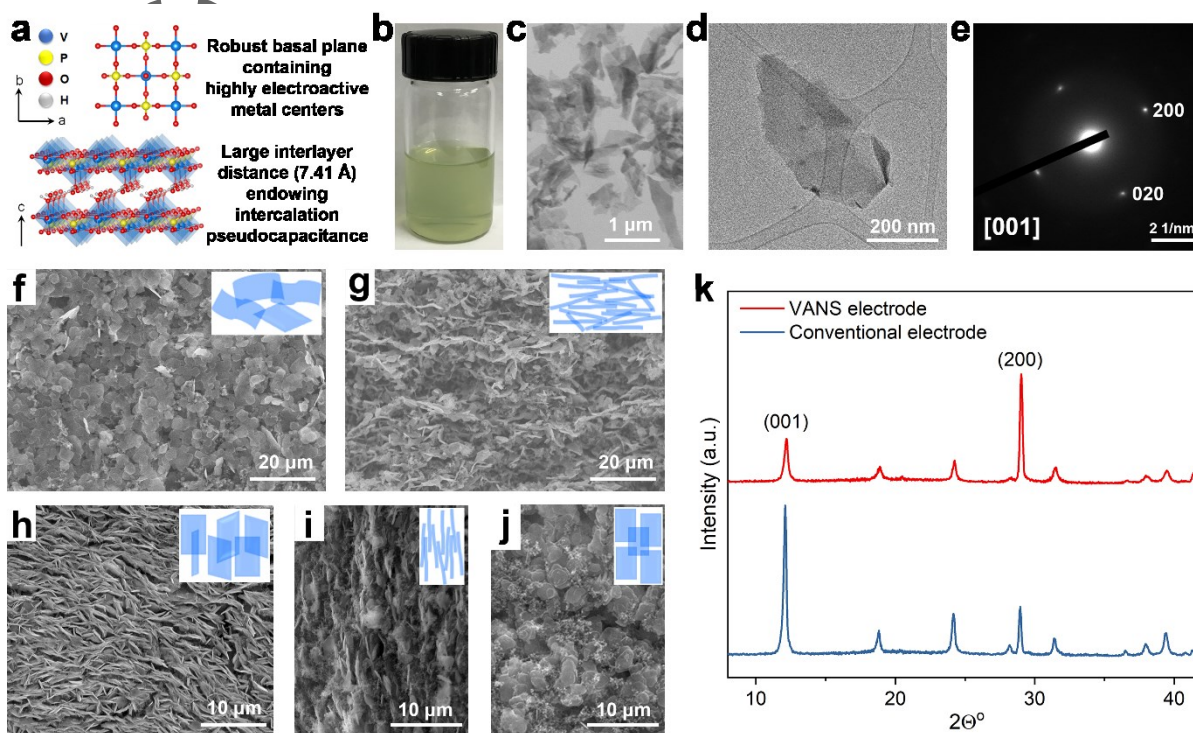


**Figure 2.** Structural characterization of  $\text{VOPO}_4$  nanosheets and nanosheet-based electrodes. a) Basic structural properties of  $\text{VOPO}_4$  material. b) Dispersion of  $\text{VOPO}_4$  nanosheets in 2-propanol after exfoliation. c) Morphology of the nanosheets. d) TEM image of an individual nanosheet and e) the corresponding SAED pattern. f) Top and g) side views of the conventional electrode. h) Top and i,j) side views of the VANS electrode. k) XRD patterns of the two electrodes showing different relative peak intensities for basal and edge planes.

The success in observed vertical alignment is a combination of using a mixed 2-propanol/water solvent in the slurry preparation and applying an intentional rapid evaporation process. Control experiments exclude the possible effect of Super P carbon additive on the alignment, as films of VOPO<sub>4</sub> nanosheets prepared without Super P exhibited similar morphologies (Figure S3, Supporting Information). In fact, the vertical alignment seems to be even better without Super P. Slow evaporation, such as air-drying and freeze-drying, failed to induce the vertical alignment (Figure S4, Supporting Information), indicating such configuration is likely a product of a kinetic process. The importance of using the mixed solvent should be emphasized as neither 2-propanol nor water alone was able to produce the VANS electrode even under rapid evaporation. However, it should be noted that in the case of pure water, the nanosheets were found to form aggregated clusters, which indeed exhibited a partially vertical aligned arrangement (Figure S5, Supporting Information). In a previous study on solvent evaporation induced self-assembly of graphene,<sup>[13]</sup> a similar solvent effect was employed and the resulted oriented arrangement was attributed to the appropriate surface tension of mixed solvent. Here, it is possible that water molecules tend to induce assembly of nanosheets into stacked clusters by interacting strongly with individual nanosheets.<sup>[14]</sup> Therefore, the critical role of water in the mixed solvent can be understood as a binder to enhance molecular interactions between the nanosheets, thereby increasing the packing density that required in the final vertical alignment.

Advanced architectures based on vertically aligned nanosheets have shown great promise for applications involving directional mass transport.<sup>[15]</sup> To demonstrate the benefit of using VANS electrodes with potentially enhanced transport kinetics, their electrochemical performance in LIBs was investigated with conventional electrodes serving as a reference. In terms of rate capability, the

conventional electrodes exhibit excellent performance with low mass loading ( $1 \text{ mg/cm}^2$ ), but the delivered capacities become lower as the loading increases ( $3$  and  $5 \text{ mg/cm}^2$ ), especially at high C rates (Figure 3a). The challenge of building thick electrodes using 2D nanosheets is clearly manifested by the significant performance loss at  $5 \text{ mg/cm}^2$ . For instance, at this high mass loading, the conventional electrode cannot be charged or discharged beyond 5 C. In contrast, the VANS electrode with  $5 \text{ mg/cm}^2$  mass loading exhibits much improved rate performance compared with the corresponding conventional electrodes (Figure 3b). In particular, its delivered capacities at high rates (5 and 10 C) are close to that of conventional electrode with  $1 \text{ mg/cm}^2$  mass loading. At low rates, the capacities are somewhat lower in the VANS electrode, indicating the contact between  $\text{VOPO}_4$  nanosheets and Super P becomes less effective as a result of orientation change. Other than that, the VANS electrode exhibits stable cycling performance at 5 C up to 1,000 cycles (Figure 3c), while the instability observed in the first few cycles is likely to be caused by insufficient electrolyte penetration in thick electrode under high C rate. The well-preserved aligned structure of the VANS electrode after cycling (Figure S6, Supporting Information) confirms its high structural stability. Despite slight thickening of the nanosheets possibly due to repeated lithiation/delithiation processes, the vertical channels for directional ion transport remains largely intact.

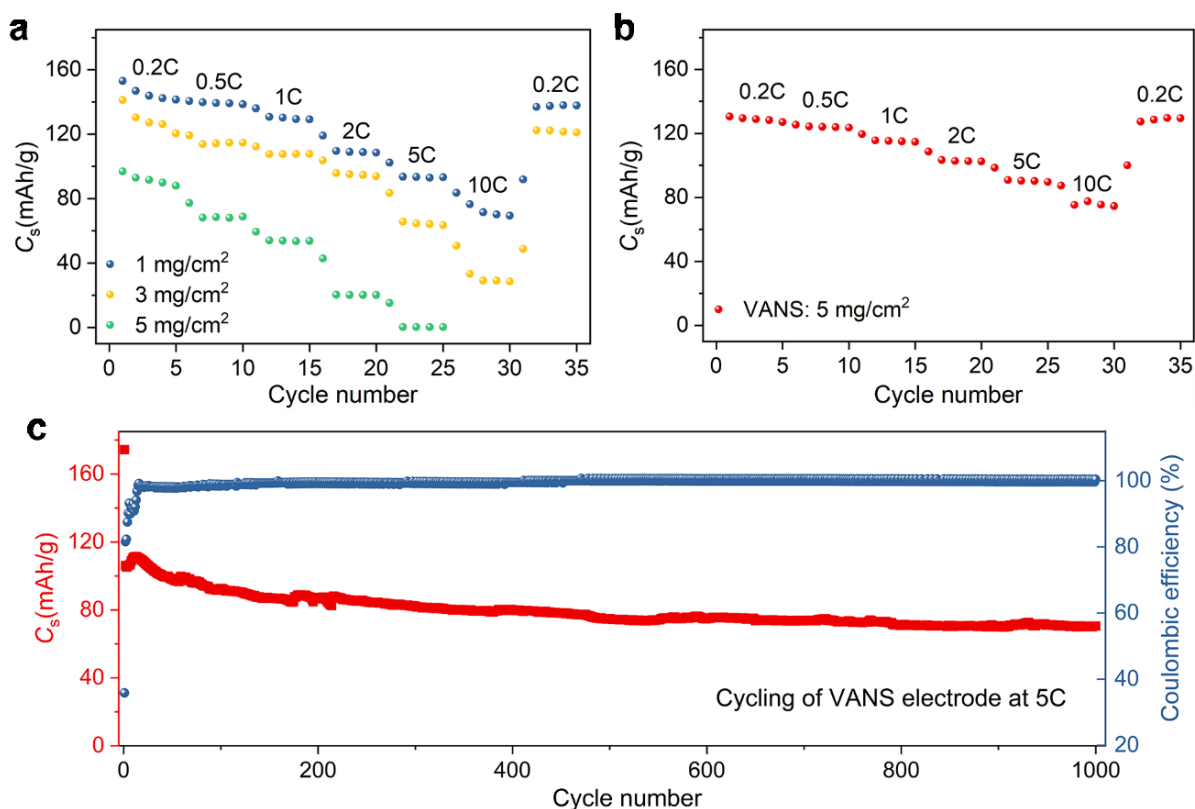


**Figure 3.** Electrochemical performance of conventional and VANS electrodes. a) Rate capability of the conventional electrodes as a function of mass loading. (b) Rate capability of the VANS electrode at 5 mg/cm<sup>2</sup>. (c) Cycling stability of the VANS electrode at 5 C.

To gain insight into charge transfer processes in the nanosheet-based electrodes, kinetic analysis using electrochemical impedance spectroscopy (EIS) was carried out during a complete charge-discharge cycle (Figure S7, Supporting Information). In the discharge process, a series of depressed semicircles at high frequency and a straight sloping line at low frequency could be observed in all electrodes (Figure S8, Supporting Information). The size of the semicircle is seen to increase slightly and then decrease to almost the original value in the 1 mg/cm<sup>2</sup> conventional electrode, which showed the best electrochemical performance. In all the other tested electrodes, a similar trend can be observed but the semicircles differ widely in size. Comparison of the Nyquist plots of all tested

electrodes, for instance at open circuit voltage (OCV), clearly indicates the existence of thickness dependent and alignment dependent charge transfer kinetics (**Figure 4a**). To quantitatively analyze the electrochemical processes, the impedance data were fitted to an appropriate equivalent circuit (Figure S9, Supporting Information) and the simulations were carried out to determine values for charge transfer resistance at various voltages with thickness taken into consideration.<sup>[16]</sup> Generally, the charge transfer resistance initially increases and then decreases in conventional electrodes (Figure 4b). The transport kinetics seems to be very poor in the one with 5 mg/cm<sup>2</sup> mass loading, as the evolution of resistance values seriously lags behind the common trend in samples with lower mass loading. In contrast, the 5 mg/cm<sup>2</sup> VANS electrode is somewhere between the two conventional electrodes with 1 and 3 mg/cm<sup>2</sup> mass loading, as well as obeying the trend observed in 1 mg/cm<sup>2</sup> conventional electrode. The results obtained from EIS measurements are also in accordance with the rate performance. The VOPO<sub>4</sub> nanosheets material has been previously demonstrated to feature a charge storage process not limited by solid state diffusion,<sup>[12b, 17]</sup> therefore, the probed charge transfer resistance here can be directly correlated to the ion transport kinetics in the electrode architecture. The increasing of charge transfer resistance in the conventional electrodes displays an adverse thickness scaling effect that limits the scalable fabrication of a thick electrode toward practical application. The reduced charge transfer resistance in the VANS electrode implies that ion transport has been enhanced in this architecture, which can be unequivocally attributed to the vertical alignment. To directly visualize the impact of nanosheets orientation on the ion transport process, two models of 600 x 450 nm nanosheet arrays with representative horizontal and vertical arrangements were constructed based on the typical lateral size and thickness of the exfoliated VOPO<sub>4</sub> nanosheets (Figure S10, Supporting Information). Dynamic diffusion of electrolyte into the nanosheet arrays under cell operation conditions were then

simulated in COMSOL. For a fixed electrochemical reaction time, the concentration profile in the VANS electrode exhibits a much deeper penetration depth compared with that in the conventional electrode (Figure 4c and d). Though the electrochemical processes were modeled with idealized geometries in a tiny volume, the results clearly demonstrate the advantageous vertical orientation that enables facilitated ion transport. The contrast is expected to be even larger in real electrodes as the diffusion channels are more distorted in the conventional electrode, in which the nanosheets are more randomly arranged.

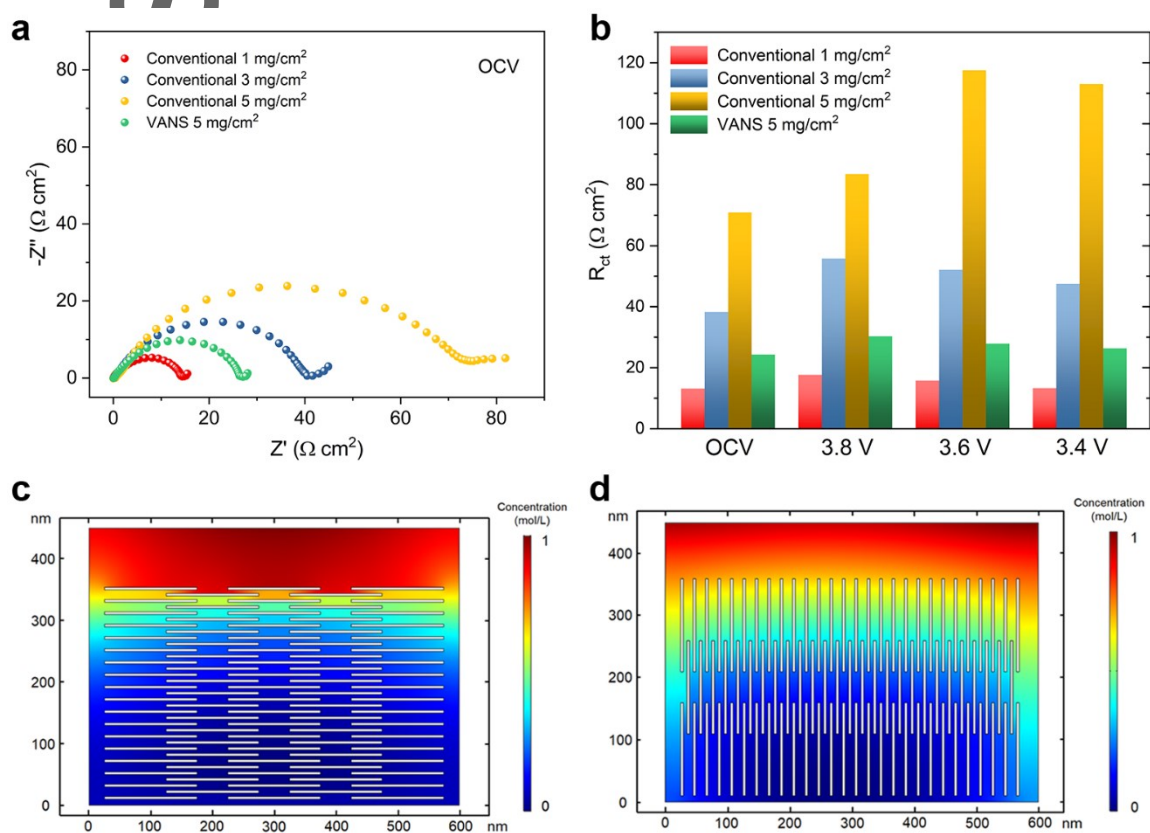


**Figure 4.** Analysis of charge transfer kinetics using EIS and simulation of ion transport in conventional and VANS electrodes. a) Nyquist plots for various electrodes at OCV. b) Comparison of charge

transfer resistance at various discharge voltages. Simulated electrolyte concentration profiles in the simplified models representing c) conventional electrode and d) VANS electrode.

The enhanced ion transport kinetics in VANS electrode is further corroborated by probing the phase transformation of the active material using in situ XRD.<sup>[18]</sup> To best differentiate the lithiation and delithiation processes between conventional and VANS electrodes, two 5 mg/cm<sup>2</sup> electrodes were subjected to two or three cycles at an intermediate charge-discharge rate of 1 C (Figure S11, Supporting Information). In both cases, the (001) peak upshifts upon discharge and returns to its original position upon charge, which relates to the reversible insertion of Li ions into the layered structure (Figure 5a and c). In addition, appearance of a permanent peak at ~16° could be spotted in the as shown second cycle, and the corresponding voltage profiles on the right again confirms a higher capacity in the VANS electrode. Two key differences are manifested in the contour plots of peak intensities (Figure b and d). First, the shift of (001) peak at fully discharged state is more significant in the VANS electrode, as highlighted by the white dashed contours. Since the position of (001) peak corresponds to the layer separation of VOPO<sub>4</sub>, and intercalation of Li-ions generally reduces the interlayer distance, larger shift of (001) peak thus indicates higher extent of intercalation. Second, the newly emerged peak after first cycle, as highlighted by the red triangles, has a much higher intensity than that of the (001) peak in the VANS electrode. If this peak belongs to a stabilized new phase after the first lithiation process, then its higher intensity implies a larger degree of initial structure conversion in the VOPO<sub>4</sub> nanosheets. Both observations conclude that, in the VANS electrode, a more complete phase transformation of the active material has been realized during electrochemical cycles. This is only possible when the ionic transport is improved in the VANS electrode as compared to the sluggish one in the conventional electrode at high mass loading. In

fact, a similar contour plots showing large peak shift can be also found in  $1 \text{ mg/cm}^2$  conventional electrode (Figure S12, Supporting Information), matching well with the previous kinetics analysis.

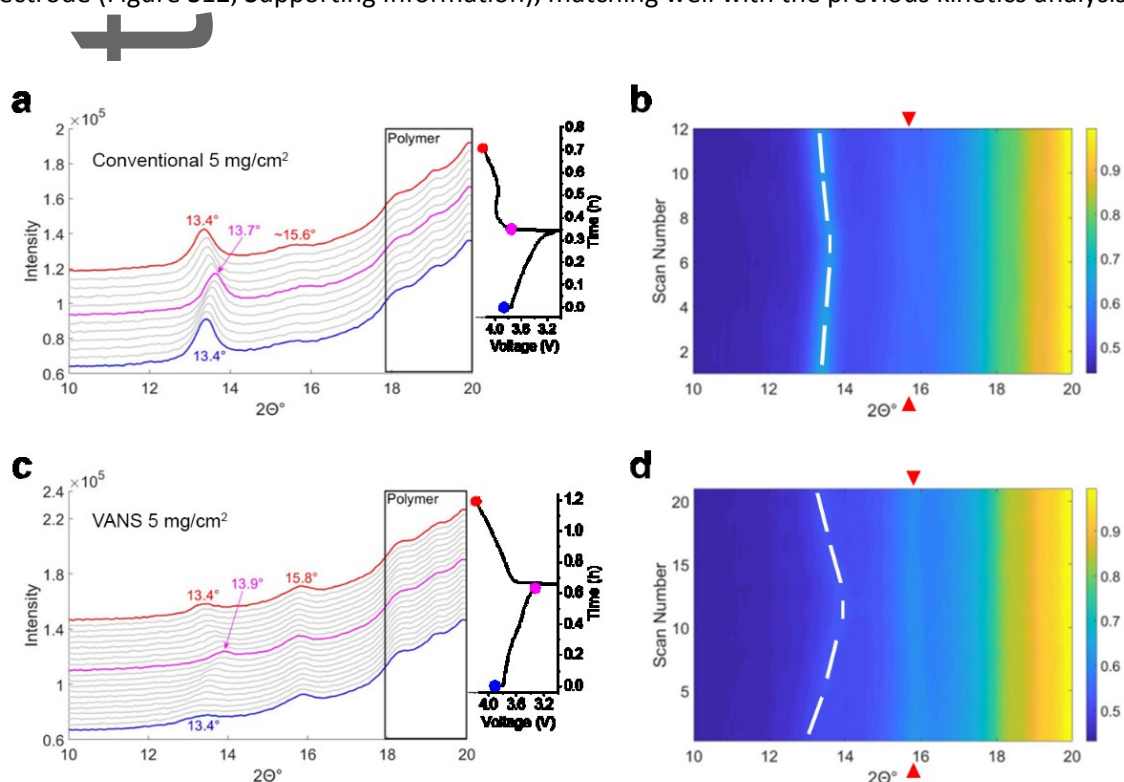


**Figure 5.** Phase transformation in  $5 \text{ mg/cm}^2$  electrodes probed by in situ XRD. a) In situ XRD patterns collected during cycling at 1 C with associated charge-discharge profiles and b) contour plot of peak intensities for  $5 \text{ mg/cm}^2$  conventional electrode. c,d) Corresponding plots for  $5 \text{ mg/cm}^2$  VANS electrode. Measurements were taken during the second cycle for both cases.

In summary, the construction of orientation-controlled nanosheet-based electrode can be achieved by a solvent evaporation induced alignment mechanism. Directional ion transport enabled by vertical alignment of nanosheets demonstrates the feasibility of mitigating performance loss due to impeded ion transport kinetics in high mass loading electrodes. In the model system based on

VOPO<sub>4</sub> material, the vertically aligned nanosheets electrode is able to deliver competitive rate performance at a high mass loading where the conventional electrode almost completely fails. The enhanced transport kinetics is well supported by the smaller charge transfer resistance and more complete phase transformation probed by in situ electrochemical and structural characterization. Besides the promising electrochemical performance, the solvent based electrode fabrication method developed in this work offers a facile yet powerful technique to build advanced electrode architectures with high density and low tortuosity, and can be readily extended to other material systems sharing the similar nanosheet morphology.

### **Supporting Information**

Supporting Information is available from the Wiley Online Library or from the author.

### **Acknowledgements**

This research was supported by the Center for Mesoscale Transport Properties, an Energy Frontier Research Center supported by the DOE-BES, under award #DE-SC0012673. D.M.L. acknowledges the support of the National Science Foundation Graduate Research Fellowship under grant no. 1839287.

### **Conflict of Interest**

The authors declare no conflict of interest.

### **Keywords**

nanosheets, solvent evaporation, vertical alignment, thick electrode, Li-ion batteries

Received: ((will be filled in by the editorial staff))

Revised: ((will be filled in by the editorial staff))

Published online: ((will be filled in by the editorial staff))

## References

- [1] a) M. Armand, J. M. Tarascon, *Nature* **2008**, *451*, 652; b) J. B. Goodenough, K.-S. Park, *J. Am. Chem. Soc.* **2013**, *135*, 1167; c) Q. Wu, C. D. Quilty, K. J. Takeuchi, E. S. Takeuchi, A. C. Marschilok, *MRS Adv.* **2018**, *3*, 1269.
- [2] a) Y. Sun, N. Liu, Y. Cui, *Nat. Energy* **2016**, *1*, 16071; b) M. R. Lukatskaya, B. Dunn, Y. Gogotsi, *Nat. Commun.* **2016**, *7*, 12647; c) E. Pomerantseva, Y. Gogotsi, *Nat. Energy* **2017**, *2*, 17089; d) L. Peng, Z. Fang, Y. Zhu, C. Yan, G. Yu, *Adv. Energy Mater.* **2018**, *8*, 1702179; e) Y. Shi, X. Zhou, G. Yu, *Acc. Chem. Res.* **2017**, *50*, 2642.
- [3] a) H. Sun, J. Zhu, D. Baumann, L. Peng, Y. Xu, I. Shakir, Y. Huang, X. Duan, *Nat. Rev. Mater.* **2019**, *4*, 45; b) Y. Kuang, C. Chen, D. Kirsch, L. Hu, *Adv. Energy Mater.* **2019**, *9*, 1901457.
- [4] a) C. Zhu, R. E. Usiskin, Y. Yu, J. Maier, *Science* **2017**, *358*, eaao2808; b) P. F. Smith, K. J. Takeuchi, A. C. Marschilok, E. S. Takeuchi, *Acc. Chem. Res.* **2017**, *50*, 544; c) X. Zhang, A. M. Bruck, Y. Zhu, L. Peng, J. Li, E. Stach, Y. Zhu, K. J. Takeuchi, E. S. Takeuchi, A. C. Marschilok, G. Yu, *Nano Futures* **2018**, *2*, 035008.
- [5] a) F. Bonaccorso, L. Colombo, G. Yu, M. Stoller, V. Tozzini, A. C. Ferrari, R. S. Ruoff, V. Pellegrini, *Science* **2015**, *347*, 1246501; b) L. Peng, Y. Zhu, D. Chen, R. S. Ruoff, G. Yu, *Adv. Energy Mater.* **2016**, *6*, 1600025; c) H. J. Lee, J. Shin, J. W. Choi, *Adv. Mater.* **2018**, *30*, 1705851; d) Y. Zhu, L. Peng, Z. Fang, C. Yan, X. Zhang, G. Yu, *Adv. Mater.* **2018**, *30*, 1706347.
- [6] a) J. Liu, X.-W. Liu, *Adv. Mater.* **2012**, *24*, 4097; b) X. Zhang, Y. Zhu, A. M. Bruck, L. M. Housel, L. Wang, C. D. Quilty, K. J. Takeuchi, E. S. Takeuchi, A. C. Marschilok, G. Yu, *Energy Storage Mater.* **2019**, *19*, 439.
- [7] a) Y. Xu, Z. Lin, X. Zhong, X. Huang, N. O. Weiss, Y. Huang, X. Duan, *Nat. Commun.* **2014**, *5*, 4554; b) H. Zhang, A. I. Cooper, *Adv. Mater.* **2007**, *19*, 1529; c) J. S. Sander, R. M. Erb, L. Li, A. Gurijala, Y. M. Chiang, *Nat. Energy* **2016**, *1*, 16099; d) H. Zhu, W. Luo, P. N. Ciesielski, Z. Fang, J. Y. Zhu, G. Henriksson, M. E. Himmel, L. Hu, *Chem. Rev.* **2016**, *116*, 9305.
- [8] a) H. Sun, L. Mei, J. Liang, Z. Zhao, C. Lee, H. Fei, M. Ding, J. Lau, M. Li, C. Wang, X. Xu, G. Hao, B. Papandrea, I. Shakir, B. Dunn, Y. Huang, X. Duan, *Science* **2017**, *356*, 599; b) L. Peng, Z. Fang, J. Li, L. Wang, A. M. Bruck, Y. Zhu, Y. Zhang, K. J. Takeuchi, A. C. Marschilok, E. A. Stach,

This article is protected by copyright. All rights reserved.

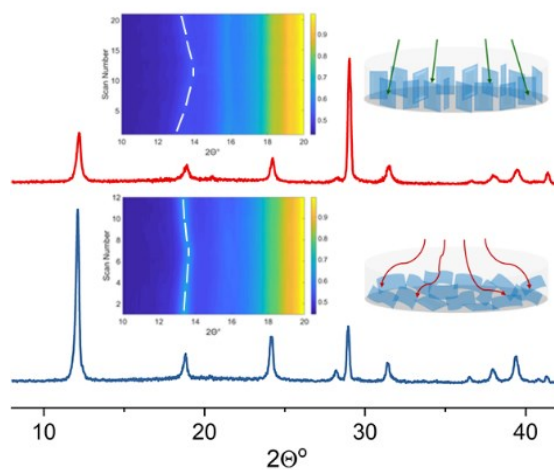
- E. S. Takeuchi, G. Yu, *ACS Nano* **2018**, *12*, 820; c) H. Ma, H. Geng, B. Yao, M. Wu, C. Li, M. Zhang, F. Chi, L. Qu, *ACS Nano* **2019**, *13*, 9161; d) X. Zhang, Z. Ju, L. M. Housel, L. Wang, Y. Zhu, G. Singh, N. Sadique, K. J. Takeuchi, E. S. Takeuchi, A. C. Marschilok, G. Yu, *Nano Lett.* **2019**, *19*, 8255.
- [9] a) Y. Yoon, K. Lee, S. Kwon, S. Seo, H. Yoo, S. Kim, Y. Shin, Y. Park, D. Kim, J.-Y. Choi, H. Lee, *ACS Nano* **2014**, *8*, 4580; b) Y. Xia, T. S. Mathis, M.-Q. Zhao, B. Anasori, A. Dang, Z. Zhou, H. Cho, Y. Gogotsi, S. Yang, *Nature* **2018**, *557*, 409; c) G. Xin, W. Zhu, Y. Deng, J. Cheng, L. T. Zhang, A. J. Chung, S. De, J. Lian, *Nat. Nanotechnol.* **2019**, *14*, 168.
- [10] C. J. Brinker, Y. Lu, A. Sellinger, H. Fan, *Adv. Mater.* **1999**, *11*, 579.
- [11] W. Wei, F. Bai, H. Fan, *Angew. Chem. Int. Ed.* **2019**, *58*, 11956.
- [12] a) C. Wu, X. Lu, L. Peng, K. Xu, X. Peng, J. Huang, G. Yu, Y. Xie, *Nat. Commun.* **2013**, *4*, 2431; b) Y. Zhu, L. Peng, D. Chen, G. Yu, *Nano Lett.* **2016**, *16*, 742.
- [13] J. Ma, X. Zhou, S. Ding, Z. Liu, *RSC Adv.* **2017**, *7*, 15469.
- [14] J.-C. P. Gabriel, F. Camerel, B. J. Lemaire, H. Desvaux, P. Davidson, P. Batail, *Nature* **2001**, *413*, 504.
- [15] a) D. Kong, H. Wang, J. J. Cha, M. Pasta, K. J. Koski, J. Yao, Y. Cui, *Nano Lett.* **2013**, *13*, 1341; b) M. Chatti, T. Gengenbach, R. King, L. Spiccia, A. N. Simonov, *Chem. Mater.* **2017**, *29*, 3092; c) L. Li, J. Gong, C. Liu, Y. Tian, M. Han, Q. Wang, X. Hong, Q. Ding, W. Zhu, J. Bao, *ACS Omega* **2017**, *2*, 1089; d) G. Wang, J. Zhang, S. Yang, F. Wang, X. Zhuang, K. Müllen, X. Feng, *Adv. Energy Mater.* **2018**, *8*, 1702254.
- [16] a) D. P. Abraham, S. Kawauchi, D. W. Dees, *Electrochim. Acta* **2008**, *53*, 2121; b) N. Ogihara, Y. Itou, T. Sasaki, Y. Takeuchi, *J. Phys. Chem. C* **2015**, *119*, 4612.
- [17] a) L. Peng, Y. Zhu, X. Peng, Z. Fang, W. Chu, Y. Wang, Y. Xie, Y. Li, J. J. Cha, G. Yu, *Nano Lett.* **2017**, *17*, 6273; b) Y. Zhu, Y. Ji, Z. Ju, K. Yu, P. J. Ferreira, Y. Liu, G. Yu, *Angew. Chem. Int. Ed.* **2019**, *58*, 17205.
- [18] N. W. Brady, Q. Zhang, A. Bruck, D. C. Bock, C. A. Gould, A. C. Marschilok, K. J. Takeuchi, E. S. Takeuchi, A. C. West, *J. Electrochem. Soc.* **2018**, *165*, A371.

Fabrication of dense and vertically aligned nanosheets-based electrodes is achieved via a controlled solvent evaporation process. The structurally advantageous architecture features excellent rate capabilities, lower charge transfer resistances and more complete phase transformation of active material, much superior to the arrangement of stacked nanosheets commonly found using the conventional electrode preparation method.

**Keywords:** nanosheets, solvent evaporation, vertical alignment, thick electrode, Li-ion batteries

Yue Zhu, Zhengyu Ju, Xiao Zhang, Diana M. Lutz, Lisa M. Housel, Yangen Zhou, Kenneth J. Takeuchi, Esther S. Takeuchi, Amy C. Marschilok, and Guihua Yu\*

### Evaporation Induced Vertical Alignment Enabling Directional Ion Transport in 2D Nanosheet-Based Battery Electrode



This article is protected by copyright. All rights reserved.